Effects of annealing temperature on the optical, bonding, structural and electrical properties of nitrogenated amorphous carbon thin films grown by surface wave microwave plasma chemical vapor deposition

M. RUSOP
Department of Environmental Technology and Urban Planning, Nagoya Institute of Technology, Gokiso-cho, Showa-ku, Nagoya 466-8555, Japan
E-mail: hambalah@gmail.com

A. M. M. OMER, S. ADHIKARI
Department of Electronic Engineering, Faculty of Engineering, Chubu University, Matsumoto-cho 1200, Kasugai 487-8501, Japan

S. ADHIKARY, H. UCHIDA
Department of Electronic Engineering, Faculty of Engineering, Chubu University, Matsumoto-cho1200, Kasugai 487-8501, Japan

T. SOGA, T. JIMBO
Department of Environmental Technology and Urban Planning, Nagoya Institute of Technology, Gokiso-cho, Showa-ku, Nagoya 466-8555, Japan

M. UMENO
Department of Electronic Engineering, Faculty of Engineering, Chubu University, Matsumoto-cho 1200, Kasugai 487-8501, Japan

Published online: 12 January 2006

We have studied the effects of annealing temperature (AT) on the properties of nitrogenated amorphous carbon (a-C:N) films grown at room temperature (RT) on quartz substrates by surface wave microwave plasma chemical vapor deposition (SWMP-CVD) using camphor alcohol gas as carbon plasma sources. The thickness, optical, bonding, structural and electrical properties of the as-grown (RT) and anneal-treated in range from 100 to 500°C of a-C:N films were measured and compared. The film thickness is decreased rapidly with increasing AT above 350°C. The wide range of optical absorption characteristics is observed depending on the AT. The optical band gap of as-grown a-C:N films is approximately 2.8 eV, gradually decreased to 2.5 eV for the films anneal-treated at 300°C and beyond that it decreased rapidly up to 0.9 eV at 500°C . Visible-Raman Spectroscopy (Raman) revealed the amorphous structure of as-grown a-C:N films and, the growth of nanocrystallinity of a-C:N films upon increase of AT. Raman and Fourier transform infrared spectroscopy (FTIR) analyses respectively shown the structural and composition of the films can be tuned by optimizing the AT. The change of optical, bonding, structural and electrical properties of SWMP-CVD grown a-C:N films with higher AT was attributed due to the fundamental changes in the bonding and band structure of the a-C:N films.
© 2006 Springer Science + Business Media, Inc.

0022-2461 © *2006 Springer Science + Business Media, Inc.*
DOI: 10.1007/s10853-005-2635-y

1. Introduction

The mostly fabricated silicon based solar cells to date are very expensive to use on a commercial basis [1, 2]. The cost reduction of solar cell and establishment of environmentally friendly production process are very important for further spread of photovoltaic technology. With respect to present high efficient solar cell materials, carbon is a material of highly stable, cheap and non-toxic which can be obtained from precursors those are sufficiently available in nature. There is a growing interest in crystalline diamond, diamond like carbon (DLC), tetrahedral carbon (ta-C), amorphous carbon (a-C), hydrogenated amorphous carbon (a-C:H) and nitrogenated amorphous carbon (a-C:N) thin films because of their well-known outstanding properties such as carbon is a material of highly stable, cheap and non-toxic which can be obtained from precursors those are sufficiently available in nature, high hardness, high electrical resistivity, high thermal conductivity, high dielectric strength, infrared transparency and optical band gap varying over a wide range from that of insulating diamond (∼5.5 eV) to that of metallic graphite (∼0.0 eV).

There have been many interests in the study of the properties of chemical vapor deposited (CVD) crystalline diamond or DLC thin films as candidate materials for future new electronic devices. For a deposition of large area (over 10 cm) crystalline diamond films, however, it is generally required a high power electromagnetic wave source, such as 2.45 GHZ microwave having up to 6 kW or 915 MHz UHF waves having up to 60 kW [3]. It is also needed to heat the substrate (over 800°C) for deposition of high quality diamond films. On the contrary, the DLC, a-C, a-C:H and a-C:N thin films can be grown on silicon substrates at relatively low temperature using various methods such as pulsed laser deposition [4–7], ion beam deposition [8, 9], sputtering [10, 11], CVD [12, 13] and r.f./microwave plasma CVD [14–19]. The low temperature CVD is a great advantage from the advantage of manufacturing aspect. Furthermore, the enlargement of DLC films required for a variety of industrial applications can be done using the large area plasma sources, such as RF discharge plasmas. Recently, another type of plasma source, known as the surface wave plasma (SWP) is also noticed as one of promising plasma sources for the large-area thin film preparation method.

The properties of a-C films known to be strongly depend on the precursor material and method of deposition. Hydrogen in a-C films modifies the properties of the films and introduces many sp^3 sites, causing an increase in the band gap [20]. Depending on the conditions and method of deposition, carbon films containing varying proportions of fourfold (sp^3)- and threefold (sp^2)-coordinated bonded a-C or a-C:H can be obtained. A tetrahedral (sp^3)-coordinated carbon atom has four inplane σ bonds while a trihedral (sp^2) has three σ bonds and one π orbital normal to the σ-bonded plane. Photon-assisted electronic transitions occur between filled bonding states (σ or π) and the empty anti bonding (σ^* or π^*) states [21]. Since π states are more weaker bonded, they lie closer to the Fermi level (E_F) than the σ states. Therefore, filled π states form valence band edges while empty π^* states form conduction band edges, and these (π and π^*) states control the size of the optical gap. The electronic properties are also control by these lower-gap bands. Therefore, the optical properties of these films are of much interest because of their potential application in semiconductor technologies including photonic devices.

To our knowledge, so far, methane or acetylene is commonly used as a precursor material in r.f./microwave plasma CVD deposition methods for the preparation of a-C thin films. However, camphor ($C_{10}H_{16}O$), a natural source, is a new precursor material thought to have an additional advantage over graphite in the sense that while the latter is purely sp^2-hybridized, the former consists of both sp^2- and sp^3- hybridized carbons in its structure. We have been working on camphor as a precursor material and generated various forms of carbon such as semiconducting a-C their possible application in light energy conversion devices [22–26]. In this paper, we report the effects of annealing temperature (AT) on the optical, bonding, structural and electrical properties of a-C:N films grown on quartz substrates by newly developed large area surface wave microwave plasma chemical vapor deposition (SWMP-CVD) using alcohol camphor as a carbon plasma source.

2. Experimental

We have developed a newly deposition method of SWMP-CVD system [27, 28] for the deposition of a-C:N thin films at low temperatures. This method is useful to avoid plasma-induced damages of the substrate surface [27, 28]. An image of experimental setup is shown in Fig. 1. The SWMP-CVD was produced in a 300 mm cylindrical vacuum chamber by introducing a 2.45 GHz microwave through a quartz window via slot antennae. In the SWMP-CVD, the microwave introduced through the slot antennae drops exponentially below the quartz window where the electron density exceeds the cutoff density [27, 28]. A high plasma density with a uniform electron density more than 10^{11} cm^{-3} was formed in the vacuum chamber and broadened in the downed stream region due to the particle diffusion. This is important for the wide range deposition of thin films such as for commercial purpose.

Film deposition was carried out on the quartz and *p*-type (100) silicon (Si) wafer substrates with a resistivity of 5–10 Ω-cm and a thickness of 350 μm. Before deposition, the substrates were cleaned before-hand by acetone and methanol for each at approximately 10 min in an ultrasonic bath, rinsed with ultra-pure water, and then dried with nitrogen blower and only for Si substrates were etched with diluted hydrofluoric acid (5%), HF:H_2O (1:10) in order to remove the resistive native oxide formed over the surface. After cleaning, the substrates

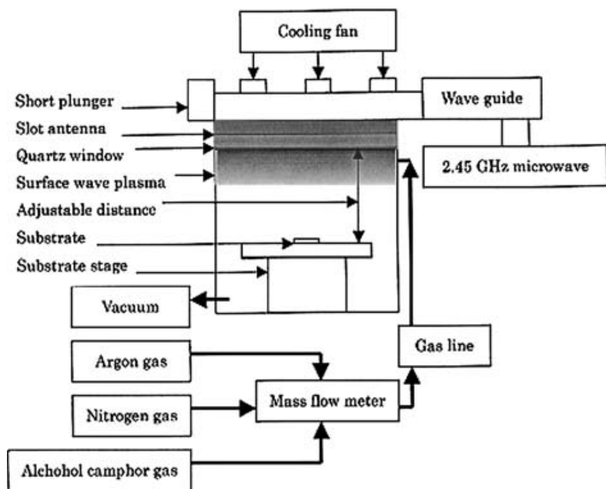

Figure 1 The schematic representation of the surface wave microwave plasma chemical vapor deposition (SWMP-CVD) system.

were quickly transferred into the chamber, placed on the substrate holder and then exposed in the chamber with Argon (Ar) plasma discharges for approximately 30 min, to etch cleaning the top surface of the substrates. The films were deposited at room temperature.

The deposition chamber was evacuated to a base pressure approximately at 3.5×10^{-4} Pa using a turbomolecular pumps for approximately 4 h and total gas pressure was fixed at 60 Pa. The launched microwave power was set approximately at 500 W. For film deposition, we have used Ar gas (Ar: 280 ml/min) as carrier gas, nitrogen gas (N_2: 5 ml/min) as dopant and camphor ($C_{10}H_{16}O$) dissolved with ethyl alcohol (C_2H_5OH) composition (CH_4: 10 ml/min), also known as camphor alcohol gas as carbon plasma sources. The chemical structure of a camphor molecule is shown in Fig. 2 [29, 30].

It has been reported that camphor has both carbon and hydrogen and moreover, it has both sp^2- and sp^3-bonded carbon in its structure [29, 30], whereas in graphite, methane or acetylene, only one type of bonding is available. The a-C:N films were grown for approximately 2 h of deposition time. The grown a-C:N films were annealed at various AT in range from 100 to 500°C in Ar gas atmosphere for 10 min and their AT effects on the optical, bonding, structural and electrical properties was analyzed by using standard experimental characterization techniques [24, 25] of scanning electron micrograph (SEM), atomic force microscopy (AFM), Nanopics 2100/NPX200 surface profiler, UV/VIS/NIR spectral reflectance and transmittance measurements, Visible-Raman scattering (Raman), Fourier transform infrared spectroscopy (FTIR) analyses and 4-point probe method of electrical measurements.

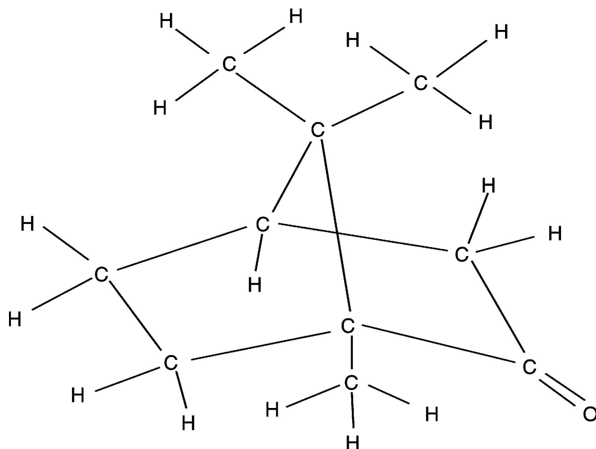

Figure 2 The chemical structure of the camphor molecule ($C_{10}H_{16}O$).

3. Results and discussions

The typical surface morphological of scanning electron microscope (SEM: Hitachi S3000H) of as grown a-C:N films is shown in Fig. 3. SEM measurement revealed that the surface morphology of the as grown films were relatively smooth and uniform. However, on some samples, a few amorphous clusters of carbon pentacle were seen. The AFM have revealed (not shown) that the film surface morphology was relatively smooth and uniform with average roughness of approximately 0.24 nm. The film thickness was measured using Nanopics 2100/NPX200 spectroscopy measurements. The average thickness of as grown (Grown temperature: 25°C) and anneal-treated a-C:N films was calculated as the measured average film thickness. Should be noted here that, when calculating the film thickness, the changes in the density and roughness of the films have not being taken into account, therefore the film thickness might become more and more over estimated as film density decreases with higher AT. As shown in Fig. 4, it has been found that the films thickness

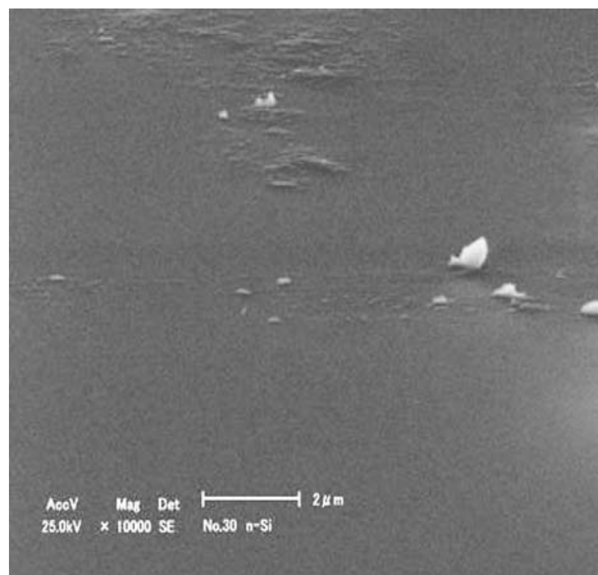

Figure 3 The scanning electron micrograph (SEM) topography image of typical as-grown (25°C) a-C:N film on silicon substrates. (Magnification: × 10 K).

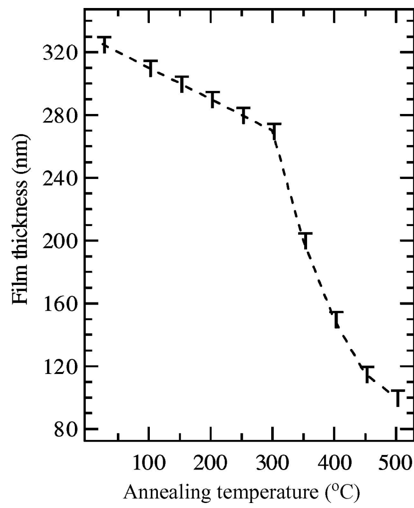

Figure 4 The film thickness as a function of annealing temperature for as-grown (25°C) a-C:N film, and a-C:N films annealed at various temperatures. (Substrate: Quartz).

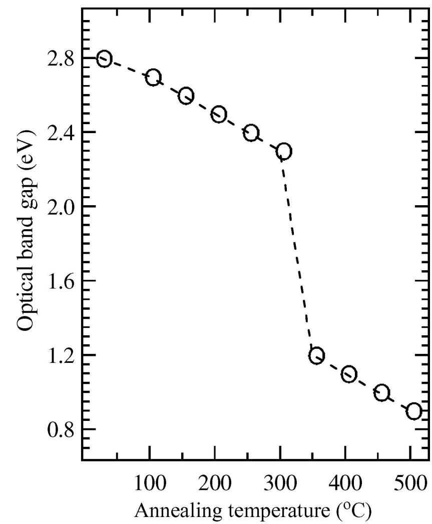

Figure 6 The optical band gap as a function of photon energy (eV) for as-grown (25°C) a-C:N film, and for a-C:N films annealed at various temperatures at (b) 100°C, (c) 150°C, (d) 200°C, (e) 250°C, (f) 300°C, (g) 350°C, (h) 400°C, (i) 450°C and (j) 500°C. (Substrate: Quartz).

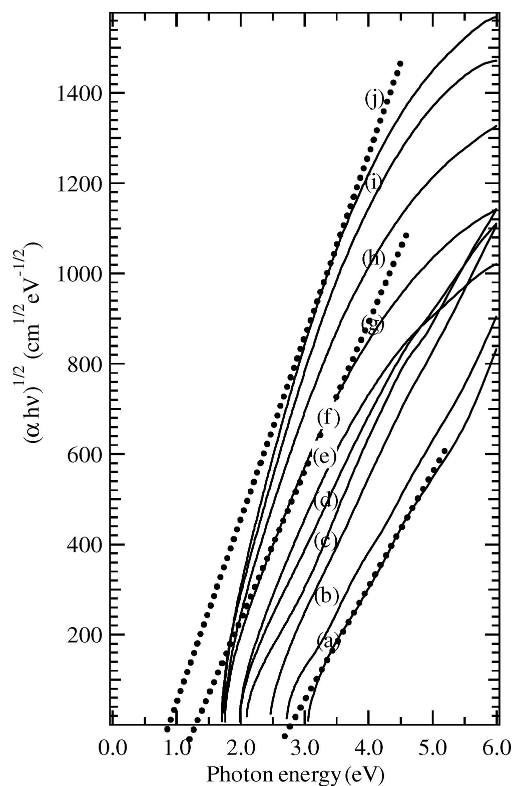

Figure 5 The Tauc plot of $(\alpha h\nu)^{1/2}$ as a function of photon energy (eV): (a) for as-grown (25°C) a-C:N film, and for a-C:N films annealed at various temperatures at (b) 100°C, (c) 150°C, (d) 200°C, (e) 250°C, (f) 300°C, (g) 350°C, (h) 400°C, (i) 450°C and (j) 500°C. (Substrate: Quartz).

is almost not depended on the AT up to 300°C, after which it decreased significantly with increasing AT.

The optical properties characterization were carried out using the as-deposited and anneal-treated a-C:N films grown on quartz substrates. The optical properties were investigated by spectral transmittance and reflectance measurements using UV/VIS/NIR spectrophotometer in range of 200–2000 nm. The Tauc optical band gap (E_g) was obtained from the extrapolation of the linear part of the curve at $\alpha = 0$ using the Tauc equation of $(\alpha \text{h}\nu)^{1/2} = B(E_g\text{-hv})$, where B is the density of the localized state constant [31]. Fig. 5 shows a plot of $(\alpha h\nu)^{1/2}$ versus photon energy, E (eV) of the films and the change of E_g as a function of annealed temperature is shown in Fig. 6. The E_g of as-grown a-C:N film was found to be approximately 2.8 eV, gradually decrease with higher AT to approximately 2.3 eV at 300°C, after which it rapidly decreased with higher AT to approximately 0.9 eV at 500°C. The variation of the optical band edge is attributed to the removal or creation of band tail states [32, 33], and the material is assumed to have less band tail states when the edge has an increase in slope. The energy (hv) dependence of α of the as-deposited and anneal-treated a-C:N films is shown in Fig. 7. From the measurements of optical reflectance and transmittance, an optical absorption coefficient (α) was calculated to be on the order of 10^3–10^5 cm^{-1}. As shown in Fig. 7, the optical absorption edges of these carbon films are broad and increase upon heat treatment, gradually increased with AT up to 300°C and rapidly increased thereafter with higher AT.

The shape of the optical absorption edge in our experiment is similar to absorption edge found in a-C:N films [33, 34]. Our results also agree with them [33, 34], that the absorption edge where it shifts towards lower photon energy (higher wavelength) region with increasing AT has a reduction in transparency. This is evident as we found that the reflectance is decreased while transmittance is observed to increase with higher AT. The decrease of E_g (Fig. 6) with higher AT above 300°C, can be related due to the structural, bonding and doping modification in the a-C:N films as has been confirmed by Raman and FTIR analyses, and also by electrical measurements that will be discussed in the next section.

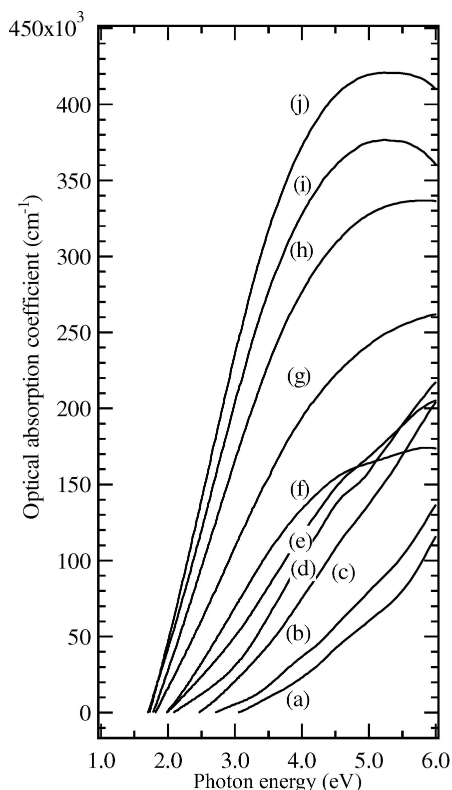

Figure 7 The optical absorption coefficient (α) plotted as a function of photon energy (eV): (a) for as-grown (25°C) a-C:N film, and (b) to (j) for a-C:N films annealed at various temperatures. (Substrate: Quartz).

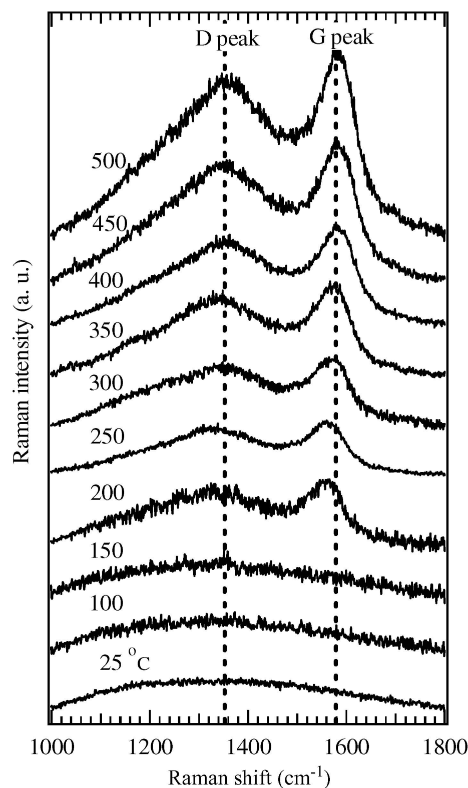

Figure 8 The Raman spectra of as-grown (25°C) a-C:N film, and a-C:N films anneal-treated at various temperatures. (Substrate: Quartz).

The α of a-C:N films is found to be similar to those of other forms of sputtered [35] and ablated [36] a-C films. A broad optical edge is observed (Fig. 7) due to the presence of localized states in mobility gap. The α increases slowly up to 300°C, and the increment is higher for higher AT. A similar trend can clearly be seen in Fig. 5, where $(\alpha h\nu)^{1/2}$ is plotted against the photon energy. The E_g is almost constant up to 300°C and a sudden decrease is observed for the films annealed at higher temperatures. From 350 to 500°C, the gradient of the optical band gap is 0.022 eV/°C with a negative sign (Fig. 6). At 500°C, the E_g is decreased to 0.9 eV. The optical absorption of the films indicates changes in the bonding and band structure. Upon heat treatment, the films become more graphitic in nature [37, 38]. Plots of optical band gap (Fig. 5) and optical absorption coefficient (Fig. 7) showed stable characteristics up to 300°C, while rapid change is observed thereafter. The change of optical properties above 300°C is might be due to the fundamental changes in the bonding and band structure of the carbon films. The details on the bonding and structural changes upon anneal-treatment are discussed elaborately in the next section through in depth Raman scattering and FTIR spectroscopy analyses.

Owing to its structural sensitivity, Raman spectroscopy is widely used for the analysis of carbon and carbon related materials [39, 40]. Raman scattering is used as a powerful technique to understand the changes of microstructural of a-C films. Raman spectra (RS) provide a wide range of structural and phase disorder information. The C–C bonding configurations were deduced from the Raman scattering spectra analysis. The analysis of such spectra is usually made by analogy with graphite [41]. Raman spectra show a main peak centered at approximately 1580 cm^{-1} (known as G peak), which corresponds to the only Raman-active mode in mono-crystalline graphite (stretching vibration mode of the C–C double bond in the plane of the hexagonal layers). While, at the low wave number is related to the disorder-induced centered approximately at 1350 cm^{-1} (known as D peak), which appears in microcrystalline or defective graphite.

Figs 8 displays the evolution of the RS in the range 1000 to 1800 cm^{-1} of as-grown and anneal-treated a-C:N films. The RS are vertically displaced for clarity, but otherwise displayed using the same scale. As can be seen from the Fig. 8, the shape and position of the spectra are almost unchanged up to 150°C, after which it gradually grows splitter in to sub band with higher AT. The G peak shifts to higher wave number and become narrower with increase of AT higher than 300°C. Thus, the Raman analyses showed that the structure of the films remain almost unaltered upon incorporation of N up to 300°C [39, 40]. The experimental result has shown the structural properties of the N-incorporated a-C:N films altered at higher AT above 300°C. As for the other component, it roughly keeps the same position and the same width while its intensity increases. Within the graphite

like model, this behavior would mean increased disorder of the sp^2-C atoms spatial arrangement. This is the reason to assigned this wide band spectra to collective vibrations of the continuously connected carbon 'skeleton' formed by both the sp^3-C and sp^2-C atoms, analogous to those occurring for tetra-coordinated amorphous semiconductors [42]. The six-fold ring-breathing mode of A_{1g} symmetry, which is forbidden in graphite but becomes active in the presence of disorder, could also contribute to this band at higher AT over 350°C [43].

The typical as-grown a-C:N films deposited at 25°C exhibited a relatively symmetric broad band, which is almost similar to those of diamond-like C (DLC) films [44, 45]. This indicated that the films had mainly a diamond-like structure. The broadband shapes of these films suggest that its structure is amorphous [44–49]. The strict selection rules for electronic transition set by the long-range translational symmetry of the crystal lattice are relaxed in amorphous state and therefore, more modes can contribute to Raman scattering resulting in the broadened RS. It has been postulated that a visible RS with a relatively symmetrical G peak corresponds to high quality of DLC film, i.e., with high sp^3/sp^2 ratio. To improve observation of the influence of AT on the detailed structure of the anneal-treated films, the experimental data were best fitted with the accuracy factor is about 0.95 by two peaks considering 2 Gaussian line shapes into two Raman bands of D and G peaks, and the linear background and the plot of this kind of RS for the as-grown and anneal-treated a-C:N films in the range of 1000 to 1800 cm^{-1} are shown in Fig. 9. From the results of deconvolution, the correlations of the Raman D and G peaks, the Raman D and G peak positions, the Raman FWHM and the intensity ratio of the Raman I_D/I_G as a function of AT are obtained from the fitting and calculated as shown in Table I. It is clear from Fig. 8, 9 and Table I that the broad band resulted from the a-C:N film (grown at 25°C) gradually splitted into two peaks (commonly known as D and G peaks) with the increase of AT, may be due to the progressive crystallization upon increase of AT. The RS shows a similar trend to those observed by Dillon *et al.* [50] and Mominuzzaman *et al.* [51] in their heat treatment experimental of C films. This indicates that these films consisted of a disordered graphite matrix with some sp^3-hybridized C states [52]. The RS indicate that a-C:N films have a graphitic structure. The variation in the position and shape of these peaks are due to the structural changes, formation of disorder, polymer rings, micro-graphite, etc., and in all cases the peaks between 1300–1400 cm^{-1} and 1500–1600 cm^{-1} are taken as evidence for the presence of a DLC in the films [53].

It is well known that these parameters are sensitive to structural changes of sp^2-hybridized C domains. As can be seen from the Figs 8, 9 and Table I, our experimental result shows that according to AT, Raman D peak intensity increases and Raman D and G peak positions shift to high wavenumber. The upward shifting of the Raman G peak position together with the increase

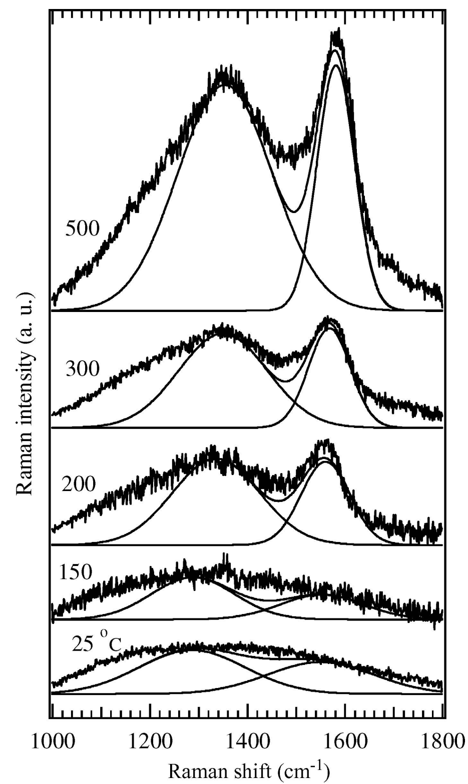

Figure 9 The Raman spectra of as-grown (25°C) a-C:N film, and a-C:N films anneal-treated at various temperatures, and their images of deconvolution of Raman D and G peaks using 2 peaks of Gaussian lines. (Substrate: Quartz).

of Raman D peak intensity is exactly the same trend as that observed from graphitization of CN films [54] and C films [55]. Raman D and G peaks gradually increases with AT up to 300°C and then rapidly shift afterwards, which shows evidence of a formation of crystallites in a-C:N films at higher AT [54]. This implies the a-C:N films are dominated by sp^2 rather than sp^3 with higher AT and which might cause the crystallites to have a bigger size [54, 55]. This phenomenon may reflect to the progress of graphitization of a-C:N films because Raman D peak is assigned to sp^2-bonded C in which seems to be aromatic in structure. An increasing in sp^2 bonding in

TABLE I The Raman fitting parameters of as-grown (25°C) a-C:N film, and a-C:N films anneal-treated at various temperatures, deconvoluted using 2 peaks of Gaussian lines

Raman parameter annealing temperature (°C)	D peak position (cm^{-1})	D peak FWHM (cm^{-1})	G peak position (cm^{-1})	G peak FWHM (cm^{-1})	I_D/I_G
25	1286.85	256.81	1550.55	256.81	1.38
150	1288.64	200.28	1553.22	200.28	1.69
200	1336.04	209.93	1560.35	117.59	1.85
300	1350.11	214.34	1568.37	101.55	1.99
500	1354.18	228.83	1581.73	90.86	2.32

these films resulted in a Raman G peak shift to a higher wave number and agree with the works of Freire Jr. *et al.* [56], Mominuzzaman *et al.* [51] and prawer *et al.* [57].

These films also followed the same trend with other authors to some extent, that is we noted here as an interesting observation that the shift of D peak is quite different from the Raman spectra of a-C films reported by several authors. Dillon *et al.* [50] observed an upward shift of D peak as a function of AT up to 400°C, which remained almost constant thereafter. Mominuzzaman *et al.* [51] observed an upward shift of D peak as a function of annealing temperature up to 400°C, which downshift rapidly thereafter. Richer *et al.* [58] observed an upward shift of D peak up to a certain value of the substrate bias where after it shifts downward but much explanation was not made for such behavior. However, as shown in Fig. 8, 9 and Table I, we have observed the shift of the G peak from about 1550 to 1580 cm^{-1}, indicates the formation of disordered nano-crystalline graphite particles, upon increase of AT. The upward shift of Raman G peak towards higher frequency, implies that the a-C:N films are dominated by sp^2 trihedral bonding rather than sp^3-tetrahedral bonding and the crystallites have a very small grain size [53]. According to our observations, the upward shift of D and G peaks in a-C:N films upon increase of AT is due to the change of bond angle disorder up to 300°C, and upward shift of D peak with rapidly upward shift of G peak at above 300°C, is due to the change in bonding (sp^3/sp^2) which in turn affects the structure of the a-C:N films.

The sp^2 structure acts as a conduction part of the amorphous network [54, 55], and the graphitic C formation is due to the presence of the sp^2 structure [56]. The upward shift of the Raman D and G peaks with increase of AT indicate the presence of the bond angle disorder [53]. The upward shift of the G peak from about 1550 to 1580 cm^{-1}, indicates the formation of disordered nano-crystalline graphite particles [51] upon increase of AT. Such a shift of D and G peaks indicate that increased of AT causes progressive graphitization in the N-incorporated a-C:N films. This may suggest that the increase of AT promotes the formation of sp^2N- C or sp^2 C-C bonding. This may can be partly explained due to the increased of collisional cooling of the ablation plume by the heavier N molecules leading to a-C:N films with more graphitic nature. Furthermore, the upshift of the Raman G peak may indicates the presence of sp^2-bonds, which is also been confirmed through FTIR analyses.

Beeman *et al.* [59] has reported about the calculations of density of state that the spectra around 1100 to 1300 cm^{-1} (D peaks) contributed from the tetragonal structures shift upward more as the sp^2 percentage increases. Upward shifting of G peaks is also from the contributions of the tetragonal (sp^2) structure. Upward shifting of this peak increases the broadening and integral density of D peaks and therefore increases the intensity ratio I_D/I_G. Dillon *et al.* [50] reported that upward shifting of the D and G peak positions could be correlated to bond angle disorder and bond length disorder. From these relations of RS, as the ST increases, the amount of sp^2-bonding increases and/or the disorder of the a-C:N films decreases. This phenomenon reflects the progress of graphitization of the a-C:N films because D peak is assigned to sp^2-bonded C, which seems to be aromatic in structure. Therefore, the upward shift of the Raman D and G peaks with increasing AT indicates the reduction of bond angle disorder and growth of graphitic domains by increase of AT.

Variations of the Raman FWHM of D and G peaks and Raman I_D/I_G also showed the growth in number and/or size of graphitic domains of a-C:N films. The Raman FWHM of G peak is related to the bond angle disorder at sp^2 sites in the C system [50]. The gradual narrowing of the G peak indicates the development of long-range order in the a-C:N films or disordering of the graphitic structure. It is clear that the Raman FWHM of D and G peaks decreases significantly upon increase of AT, which indicate the increases of the crystallinity [60]. As can be seen from Figs 8 and 9, it was obvious that the increase in AT reduced the Raman FWHM of D and G peaks. The narrowing of G peak with the increase in ST suggested the increase in graphitization in the C-C phase of the deposited films, which was similar to that in DLC films [50, 51, 56, 57, 61]. The position of the Raman D and G peaks shift to a higher frequency and the decrease of Raman FWHM of D and G peaks showed that the N incorporated in a-C:N films with increasing the AT favor the formation of sp^2 units according to Raman data.

Beeman *et al.* [59] also has reported about the upward shifting of D peak increases the broadening and integral density of D peaks and therefore increases the intensity ratio of Raman I_D/I_G. As can be seen from Fig. 9 and Table I, the Raman I_D/I_G ratio of as-grown a-C:N film (1.38) gradually increases to 1.85 with increasing of AT at 200°C and increases up to 1.99 at 300°C, which reflected the fact that the degree of disorder increased in the films. Raman I_D/I_G increases rapidly with further increase in AT over 300°C up to 2.32 at 500°C. The Raman I_D/I_G reflects the number and/or size of graphitic domains for a-C materials [50, 62, 63]. Several authors reported about the relationship between Raman I_D/I_G and structure of a-C. They reported the I_D/I_G varies inversely with the size of sp^2C crystallites [64] and the increase of Raman I_D/I_G was caused by the increase in the dimensions of graphite crystallites (sp^2 cluster size) [50] in C films. Because D peak represents a more disordered structure with very small sp^2 domains [49] and a higher amount of sp^3-hybridized C [65] whereas the G band is assigned indicative of large graphite-like sp^2 domains, this rapid increase of the I_D/I_G ratio indicates that the C matrix changes from a more graphite-like to a predominantly disordered network-like structure with further increase of AT above 300°C. The high Raman I_D/I_G ratio may be indicative of a high degree of structural disorder.

Here, we assigned the increase of Raman I_D/I_G with increasing of AT indicates that the growth of graphitic domains, i.e. graphitization by increase of AT. These micro-

structural modifications may account for the decrease in the average coordination number and the reduction in the internal stress of these films. This is may be due to the fact that high AT can promote the migration and rearrangement of particles by thermal energy during anneal-treated of a-C:N films. Raman scattering analyses have revealed the amorphous nature of C and growth of nano-crystallinity upon increase of AT. The intensity of D peak increases with increasing ST over 300°C, which implies that the films anneal-annealed at higher AT (over 300°C) contain relatively lower sp^3-bonded DLC. The Raman I_D/I_G of the as-grown a-C:N films at 25°C is lower than that of a-C:N films at 500°C. The high relative intensity ratio of Raman I_D/I_G can be correlated with the smaller band gap (Fig. 6) in DLC [56]. The relative intensity ratio of Raman I_D/I_G can be used as a parameter for sp^3 content, a smaller Raman I_D/I_G ratio corresponding to higher sp^3 content [66]. We found, the smaller Raman I_D/I_G and the larger band gap at 25°C revealed more diamond-like nature and hence more sp^3-bonded structure, which decreases at higher AT.

We found the increased of Raman D and G peak and the Raman I_G/I_G, and the decreased of Raman FWHM with the increased of AT, which may indicate that N incorporated a-C:N films caused an increase in the number and/or size of graphitic domains with higher AT. Simultaneously, transformation of C atoms from sp^3-hybridization to sp^2-hybridization takes place. These results support the theoretical model of Beeman *et al.* [67] where they have predicted downshift of G peak with increase of sp^3 fraction. In general, the electrical properties are determined by the ratio of sp^3/sp^2-hybridized C in a-C. Therefore C film with large sp^3 fraction will exhibit a high electrical resistivity similar to diamond. Hauser *et al.* [68] suggested that DLC film contains a mixture of diamond (sp^3-C bond) and graphite (sp^2-C bond) bonds, and the latter acts as a localized conduction state. Therefore, the electrical resistivity of a-C film is determined by the ratio of sp^3/sp^2-hybridized C.

The electrical resistivity (ρ) was measured at room temperature (RT) by a 4-point probe resistance measurement method, the usual way for high resistance measurement. The ρ values for each film were the average of measurements made at different positions on the film surface. Fig. 10 shows the ρ values of as-grown a-C:N film measured to be around 7.5×10^5 ($\Omega-^{cm}$) gradually decreases with higher AT to 6.1×10^5 ($\Omega-^{cm}$) at 100°C. As AT increases, the ρ decreases up to 3.5×10^5 ($\Omega-^{cm}$) at 200°C. At higher AT, as can be seen in Figs 6 and Fig. 10, both of the E_g and$\rho$are gradually decreases up to 2.3 eV and 2.3×10^5 ($\Omega-^{cm}$) at 300°C, respectively. The variation of the optical and electrical properties can be related to interstitial doping of N in a-C films through modifications of C-N bonding configurations by rearranging of N atoms upon increase of AT. However with further increase of AT above 300°C, both E_g and ρ are drastically decreases up to 0.9 eV and 1.5×10^4 ($\Omega-^{cm}$) at 500°C, respectively. This is probably due to the graphitization of the a-C:N films. Perhaps the doping of N accompanied by increase of AT above 300°C increases crystallinity and subsitutional doping of N thereby sharply decreases resistivity. These phenomena also supported by the Raman and FTIR spectroscopy measurements.

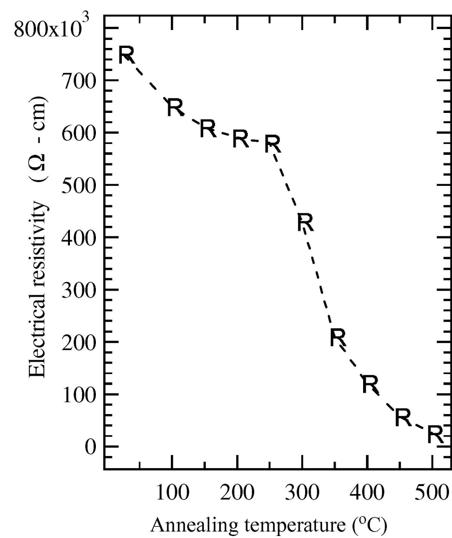

Figure 10 The variation of electrical resistivity of as-grown (25°C) a-C:N film, and a-C:N films anneal-treated at various temperatures. (Substrate: Quartz).

The bonding states of carbon (C), nitrogen (N) and hydrogen (H) atoms can be characterized by FTIR measurements. The FTIR spectra of a-C:N films has been reported by several authors. It has been reported that, Band 1 at around 700 cm^{-1} is due to the out-of-plane bending mode for the graphite-like domain [69]. The peak at around in range 1000–1360 cm^{-1} (Band 2) can be assigned to C–N and C=N bonds and the broad band extending in range 2800–3000 cm^{-1} (Band 3) corresponds to different C-H configurations [70, 71]. Broad absorption band 2 indicates that the films structure is predominantly amorphous with sp^2-C vibration modes, and is related to Raman active D modes [72]. The contributions around 1350 and 1550 cm^{-1} were initiated from disordered (D band) represents disordered sp^2-C with an amount of sp^3-C and graphite-like (G band) represents sp^2-C bonds in the a-C:N films, respectively [73]. Another contribution at around 1145–1265 cm^{-1}, was due to symmetric tetrahedral CN bond [74, 75]. According to Kaufman *et al.* [76], these Raman active D and G modes become IR active due to the incorporation of N atoms into C network that results in the symmetry breaking of the C network. Band 4 at 1100–1400 cm^{-1}, band 5 at 1500–1700 cm^{-1} and band 6 at around 2200 cm^{-1} are due to C–N, C=C and/or C=N and C—N stretching vibration modes, respectively [77, 78]. The FTIR absorption for C-H stretching vibrations on sp^2-C is found in the 2950–3060 cm^{-1} range, while for sp^3-C in the range 2850–2945 cm^{-1} range [79] and the peaks around 2926 and 2956 cm^{-1} are the most prominent, assigned to –$CH_2 sp^3$ asymmetric and –$CH_2 sp^2$ olefinic bonds respectively, and the peaks around 2855 cm^{-1} indicate the formation of sp^3 bonding [80].

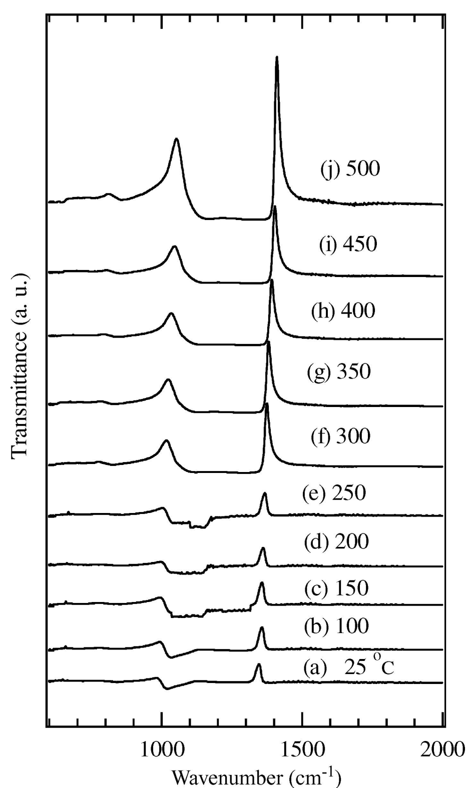

Figure 11 The FTIR spectra of as-grown (25°C) a-C:N film, and a-C:N films annealed at various temperatures. (Substrate: Quartz).

Fig. 11 shows the FTIR transmittance spectra measured in the wave number in range from 600 to 2000 cm^{-1} for as-grown and anneal-treated a-C:N films. FTIR spectra show for a-C:N films, contributions around 1350 and 1550 cm^{-1} were initiated from disordered (D band) and graphite like (G band) attributed to CN bonds [81]. Another contribution, around 1212–1265 cm^{-1}, was due to symmetric tetrahedral CN bond [82]. The broad band 1 to band 6 are appeared in all of the sample as-grown and anneal-treated a-C:N films. The absorption peak at around 2350 cm^{-1}, which is also observed in as-grown and anneal-treated a-C:N films, can be attributed to the CO_2 stretching mode arising from oxygen contamination at the film surface [83]. FTIR spectra indicated that as AT increased higher than 300°C, the intensity of the band 2 and the three characteristic peaks of DLC peaks (not shown) in the region 2800–3000 cm^{-1} peaks (Band 3) become more and more prominent suggests the formation of crystalline structure in the films [84]. The absence of clear appearance of peaks in the as-grown and a-C:N films up to 300°C suggests the amorphous nature of the films. The different of intensity of band 2 may indicates there is a different modification of the binding geometry, that is likely to induced by the increase of internal film stress arising from the increase of the trigonal bond density due to increase of AT. FTIR shows the crystalline structure of the films increases with the increases of AT over 300°C. This is evident that the composition of the films can be tuned by optimizing the AT.

The D band (1350 cm^{-1}) and G band (1550 cm^{-1}) are gradually increased with higher AT. Above 300°C, the D band seems to be gradually suppressed. This indicates no modification of the binding geometry at lower AT up to 300°C and a modification of the binding geometry with the transformation of the sp^3 C—N bonds into sp^2 C—N binding state as AT increased up to 500°C. As can be seen from Fig. 9, the single broad band of anneal-treated a-C:N films, centered at around 1350 cm^{-1} has gradually suppressed and shifted to a higher wave number and reached to about 1412 cm^{-1} at 500°C. This red shift indicates there is a modification of the binding geometry, that is likely to induced by the increase of internal film stress arising from the increase of the trigonal bond density due to increase of AT. In our spectra, bands 1, 2, 3, 4 (sp^3C—N tetrahedral), band 5 (sp^2C—N trihedral) and band 6 of as-grown and anneal-treated a-C:N films are weak and as AT increases, starting from around 300°C the intensity of broad absorption band 2 has gradually increased. This indicates the component modification of the C–N, C=N, C =C and C≡N bonds increases with higher AT above 300°C, which is also confirmed by the optical and Raman analyses. The FTIR spectra thus indicated the transformation to the graphite-like sp^2 C–N bonds and crystalline structure of the a-C:N films increases with the increase of AT above 300°C.

These characteristics resemble the properties of a-C:H films previously studied by others [16–20] and therefore, indicate the presence of hydrogen in our as-deposited a-C:N films. The possible explanation for the presence of hydrogen in our a-C:N films, can be derived from the structural properties of precursor materials, camphor ($C_{10}H_{16}O$) (Fig. 2) that was dissolved with ethyl alcohol (C_2H_5OH) composition as source gases, which differs from other precursor material in the sense that has a large amount of hydrogen in its structure. Also, it is reported that at higher temperature above 400°C, the hydrogen in the film effuses and hydrogen bonded sp^3 carbon converts to C=C-carbon sp^2 carbon [37] which in turn affects various optoelectrical properties of carbon films, as can be seen in our a-C:N films at higher anneal temperature above 300°C. Based on these observations, we suggest that precursors similar to camphor, in the sense that they contain both sp^2-and sp^3-bonded carbon in their structure, may be better and suited candidates as starting materials for semiconducting carbon for electronic applications. Also, camphor has the additional advantage that it can be used as a precursor in both physical [4–11] and chemical vapor deposition such as SWMP-CVD.

4. Conclusions

The hydrogenated amorphous carbon (a-C:N) films have been grown by surface wave microwave plasma chemical vapor deposition (SWMP-CVD) method and the effects of AT in range from 25 to 500°C has been investigated. The thickness, optical, structural and bonding properties of the

as-grown and anneal-treated a-C:N films were measured and compared. The film thickness is decreased rapidly with increasing AT above 300°C. The optical band gap of the as-grown a-C:N films was found to be approximately 2.8 eV, remained almost constant until 300°C, and beyond that it decreased monotonically up to 0.9 eV at 500°C. Raman scattering analyses revealed the amorphous structure of a-C:N films deposited at 25°C and, the growth of nanocrystallinity of a-C:N films upon increase of AT. We found that, both the sp^2 and sp^3-hybridized C atoms can be bound to the N atoms in the a-C:N films. The FTIR spectroscopy measurements also have shown that the structural and composition of the films can be tuned by optimizing the AT. The change of optical, bonding, structural and electrical properties of SWMP-CVD grown a-C:N films with higher AT was attributed due to the fundamental changes in the bonding and band structure of the films. The result shows it is possible to control optical band gap of SWMP-CVD grown a-C:N films by the annealing process for getting suitable optical band gap of solar cell application.

Acknowledgments

This work was supported by New Energy and Industrial Technology Development Organization (NEDO) under Ministry of Economy, Trade and Industry (METI), Government of Japan. A.M.M. Omer is grateful to ASJA International for its financial support and S. Adhikari is also thankful for the scholarship given by Kyoritsu International Foundation.

References

1. Z. Q. MA and B.X. LIU, *Sol. Energy Mater. Sol. Cells* **69** (2001) 339.
2. Z. B. ZHOU, R. Q. CUI, Q. J. PANG, G. M. HADI, Z. M. DING and W. Y. LI, *ibid.* **70** (2002) 487.
3. M. FUNER, C. WILD and P. KOIDL, *Appl. Phys. Lett.* **72** (1998) 1149.
4. K. YAMAMOTO, Y. KOGA, S. FUJIWARA and F. KOKAI, *Jpn. J. Appl. Phys.* **36** (1997) L1333.
5. H. J. SCHEIBE and B. SCHULTRICH, *Thin Solid Films* **246** (1994) 92.
6. D. T. PEELER and P. T. MURRAY, *Diamond Relat. Mater.* **3** (1994) 1124.
7. F. Y. CHUANG and C. Y. SUN, *Appl. Phys. Lett.* **69** (1996) 3504.
8. J. U. OH, K-R LEE and K. Y EUN, *Thin Solid Films* **270** (1995) 173.
9. V. PALSHIN, E. I. MELETIS, S. VES and S. LOGOTHETIDIS, *ibid.* **270** (1995) 165.
10. M. VOGEL, O. STENZEL, R. PETRICH, G. SCHAARSCHMIDT and W. SCHARFF, *ibid.* **227** (1993) 74.
11. N. SAVVIDES and B. WINDOW, *J. Vac. Sci. Technol.* **A 3** (1985) 2386.
12. H. A. YU, Y. KANEKO, S. YOSHIMURA and S. OTANI, *Appl. Phys. Lett.* **68** (1996) 547.
13. M. UCHIDA, H. TANAKA and K. KOTERA, *Jpn. J. Appl. Phys.* **35** (1996) 5815.
14. B. DISCHLER, A. BUBENZER and P. KOIDL, *Appl. Phys. Lett.* **42**(1983) 636.
15. RUSLI, G. A. J. AMARATUNGA and S. R. P. SILVA, *Thin Solid Films* **270** (1995) 160.
16. J. ROBERTSON, *J. Non-Cryst. Solids* **164** (1993) 1115.
17. M. MATSUOKA and K. ONO, *Appl. Phys. Lett.* **50** (1987) 1864.
18. S. MATSUO and M. KIUCHI, *Jpn. J. Appl. Phys.* **22** (1983) L210.
19. Y. H. SHING and F. S. POOL, *Vacuum* **41** (1990) 1368.
20. B. DISCHLER, A. BUBENZER and P. KOIDL, *Solid State Commun.* **48** (1983) 105.
21. J. BESOLD, R. THIELSCH, N. MATZ, C. FRENZEL, R. BORN and A MOBIUS, *Thin Solid Films* **293** (1997) 96.
22. K. M. KRISHNA, T. SOGA, K. MUKHOPADHYAY, M. SHARON and M. UMENO, *Sol. Energy Mater. Sol. Cells* **48** (1997) 25.
23. M. RUSOP, S. M. MOMINUZZAMAN, X. M. TIAN, T. SOGA, T. JIMBO and M. UMENO, *Applied Surf. Sci.* **197** (2002) 542.
24. M. RUSOP, S. M. MOMINUZZAMAN, T. SOGA, T. JIMBO and M. UMENO, *Int. J. Mod. Phys.* **B 6** (2002) 866.
25. M. RUSOP, X. M. TIAN, T. SOGA, T. JIMBO and M. UMENO, *Mol. Cryst. Liq. Cryst.* **388** (2002) 509.
26. S. M. MOMINUZZAMAN, K. M. KRISHNA, T. SOGA, T. JIMBO and M. UMENO, *Jpn. J. Appl. Phys.* **38** (1999) 658.
27. M. NAGATSU, T. SANO, N. TAKADA, N. TOYODA, M. TANGA and H. SUGAI, *Diamond Relat. Mater.* **11** (2002) 976.
28. M. NAGATSU, G. XU, I. GHANASHEV, M. KHANOH, H. SUGAI, *Plasma Sources Sci. Technol.* **6** (1997) 427.
29. K. MUKHOPADHYAY, K. M. KRISHNA and M. SHARON, *Phys. Rev. Lett.* **72** (1994) 3182.
30. M. SHARON, K. MUKHOPADHYAY, I. MUKHOPADHYAY and K.M. KRISHNA, *Carbon* **33** (1995) 331.
31. J. TAUC, “Amorphous and Liquid Semiconductors” (Plenum Press, London, New York, 1974) Chap. 4.
32. X. SHI, L. K. CHEAH and B. K. TAY, *Thin Solid Films* **312** (1998) 166.
33. L. K. CHEAH, X. SHI, J. R. SHI, E. J. LIU and S. R. P. SILVA, *J. Non-Cryst. Solids* **242** (1998) 40.
34. X. SHI, L. K. CHEAH and B. K. TAY, *Thin Solid Films* **312** (1998) 166.
35. M. YOSHIKAWA, N. NAGAI, M. MATSUKI, H. FUKUDA, G. KATAGIRI, H. ISHIDA and A. ISHITANI, *Phys. Rev B* **46** (11) (1992-I) 7169.
36. S. M. MOMINUZZAMAN, K. M. KRISHNA, T. SOGA, T. JIMBO and M. UMENO, *Jpn. J. Appl. Phys.* **38** (1999) 658.
37. M. A. TAMOR and W. C. VASELL, *J. Appl. Phys.* **76**(6) (1994) 3823.
38. B. DISCHLER, A. BUBENZER and P. KOIDL, *Appl. Phys. Lett.* **42**(8) (1983) 636.
39. D.S. KNIGHT and W. B. WHITE, *J. Mater. Res.* **4** (1989) 385.
40. S. R. P. SILVA, J. ROBERTSON, G. A. J. AMARATUNGA, B. RAFFERTY, L. M. BROWN, J. SCHWAN, D. F. FRANCESCHINI and G. MARIOTTO, *J. Appl. Phys.* **81** (1997) 2626.
41. M.A. TAMOR and W. C VASSELL, *ibid.* **76** (1994) 3823.
42. J. E. SMITH JR., M. H. BRODSKY, B. L. CROWDER, M. I. NATHAN and A. PINCZUK, *Phys. Rev. Lett.* **26** (1971) 642.
43. A.C. FERRARI and J. ROBERTSON, *Phys. Rev.* B **61** (2000) 14095.
44. P. GONZALEZ, R. SOTO, B. LEON, M. PEREZ-AMOR and T. SZORENYI, *Appl. Surf. Sci.* **154** (2000) 454.
45. P. HAMMER, M. A. BAKER, C. LENARDI and W. GISSLER, *Thin Solid Films* **290** (1996) 107.
46. A. BOUSETTA, M. LU, A. BENSAOLA and A. SCHULTS, *Appl. Phys. Lett.* **65** (1994) 696.
47. Z. J. ZHANG, S. FAN and C. M. LIEBER, *ibid.* **66** (1995) 3582.
48. W. T. ZENG, E. BROITMAN, N. HELLGREN, K. Z. XING, I. IVANOV, H. SJOSTROM, L. HULTMAN and J. E. SUNDGREN, *Thin Solid Films* **308** (1997) 223.
49. J. F. KAUFMAN, S. METIN and D. D. SAPERSTEIN, *Phys. Rev.* B **39** (1989) 13053.

50. R. O. DILLON, J. A. WOOLLAM and V. KATKANANT, *ibid.* **29** (1984) 3482.
51. S. M. MOMINUZZAMAN, K. M. KRISHNA, T. SOGA, T. JIMBO and M. UMENO, *Carbon* **38** (2000) 127.
52. Y. K. YAP, S. KIDA, T. AOYAMA, Y. MORI and T. SASAKI, *Appl. Phys. Lett.* **73** (1998) 7.
53. H. C. BARSHILIA, S. SAH, B. R. MEHRA, V. D. VANKAR, D. K. AVASTHI and G. K. MEHTA, *Thin Solid Films* **258** (1995) 123.
54. N. C. CHO, D. K. VEIRS, J. W. AGER, M. D. RUBIN, C. B. HOOPER and D. B. BOGY, *J. Appl. Phys.* **71** (1992) 2243.
55. F. L. FREIRE JR., C. A. ACHETE, G. MARIOTTO and R. CANTERI, *J. Vac. Sci. Technol.* A **12** (1994) 3048.
56. F. L. FREIRE and D. F. FRANCESCHINI, *Thin Solid Films* **293** (1997) 236.
57. S. PRAWER, K. W. NUGENT, Y. LIFSHITZ, G. D. LEMPERT, E. GROSSMAN, R. KALISH and Y. AVIGAL, *Diamond Related Mater.* **5** (1996) 433.
58. F. RICHTER, K. BEWILOGUA, H. KUPTER, I. MUHLING, B. RAU, B. ROTHER and D. SCHUMACHER, *Thin Solid Films* **212** (1)(1992) 245.
59. D. BEEMAN and J. SILVERMAN, *Phys. Rev.* B **5** (1972) 4951.
60. B. DORFMAN, M. ABRAIZOV, F. H. POLLAK, D. YAN, M. STRNGIN, X. Q. YANG and Z.Y. RONG, *Mater. Res. Soc. Symp. Proc.* **349** (1994) 547.
61. F. RICHTER, K. BEWILOGUA, H. KUPTER, I. MUHLING, B. RAU, B. ROTHER and D. SCHUMACHER, *Thin Solid Films* **212**(1) (1992) 245.
62. J. SCHWAN, S. ULRICH, V. BATORI, H. EHRHARDT and S.R.P. SILVA, *J. Appl. Phys.* **80** (1996) 440.
63. R. KALISH, Y. LIFSHITZ, K. NUGENT and S. PRAWER, *Appl. Phys. Lett.* **74** (1999) 2936.
64. D. S. KNIGHT and W. B. WHITE, *J. Mater. Res.* **4** (1989) 385.
65. M. A. BAKER and P. HAMMER, *Surf. Interf. Anal.* **25** (1997) 629.
66. M. A. TAMOR, J. A. HAIRE, C. H. WU and K. C. HASS, *Appl. Phys. Lett.* **54** (1989) 123.
67. D. BEEMAN, J. SILVERMAN, R. LYNDS and M. R. ANDERSON, *Phys. Rev.* B **30**(2) (1984) 870.
68. J. J. HAUSER, *J. Non-Cryst. Solids* **23** (1977) 21.
69. N. NAKAYAMA, Y. TSUCHIYA, S. TAMADA, K. KOSUGE, S. NAGATA, K. TAKAHIRO and S. YAMAGUCHI, *Jpn. J. Appl. Phys.* **32** (1993) 1465.
70. A. BOUSETTA, M. LU, A. BENSAOLA and A. SCHULTS, *Appl. Phys. Lett.* **65** (1994) 696.
71. Z. J. ZHANG, S. FAN and C. M. LIEBER, *ibid.* **66** (1995) 3582.
72. W. T. ZENG, E. BROITMAN, N. HELLGREN, K. Z. XING, I. IVANOV, H. SJOSTROM, L. HULTMAN and J. E. SUNDGREN, *Thin Solid Films* **308** (1997) 223.
73. P. HAMMER, M. A. BAKER, C. LENARDI and W. GISSLER, *J. Vac. Sci. Technol.* A **15** (1997) 107.
74. M. WIXOM, *J. Am. Ceram. Soc.* **73** (1990) 1973.
75. Y. TAKI, T. KITAGAWA and O. TAKAI, *Thin Solid Films* **304** (1997) 183.
76. J. F. KAUFMAN, S. METIN and D. D. SAPERSTEIN, *Phys. Rev.* B **39** (1989) 13053.
77. Y. AOI, K. ONO and E. KAMIJO, *J. Appl. Phys.* **86** (1999) 2318.
78. X. A. ZHAO, C. W. ONG, Y. C. TSANG, Y. W. WONG, P. W. CHAN and C. L. CHOY, *Appl. Phys. Lett.* **66** (1995) 2652.
79. Y. TANABE, G. BURKHARD, T. ISHIKURA, K. TSUNODA, H. HASUO, M. TAMURA, H. TAMURA, A. SAWAOKA and K. UEMATSU, *Jpn. J. Appl. Phys.* **33** (1994) 6684.
80. H. C. BARSHILA, S. SAH, B. R. MEHTA, V. D. VANKAR D. K. AVASTHI and G. K. MEHTA, *Thin Solid Films* **258** (1995) 123.
81. P. HAMMER, M. A. BAKER, C. LENARDI and W. GISSLER, *J. Vac. Sci. Technol.* A **15** (1997) 107.
82. M. R. WIXOM, *J. Am. Ceram. Soc.* **73** (1990) 1973.
83. S. L. SUNG, C. H. TSENG, F. K. CHIANG, X. J. GUO and X. W. LIU, *Thin Solid Films* **340** (1999) 169.
84. V. PAILLARD, P. MELINON, V. DUPUIS, J. P. PEREZ, A. PEREZ and B. CHAMPAGNON, *Phys. Rev. Lett.* **71** (1993) 4170.

Received 22 August 2004
and accepted 27 May 2005